Applied Catalysis B: Environmental 185 (2016) 133–140

Contents lists available at ScienceDirect

Applied Catalysis B: Environmental

journal homepage: www.elsevier.com/locate/apcatb

Au-decorated GaOOH nanorods enhanced the performance of direct methanol fuel cells under light illumination

Yi-Han Hsu [1], An T. Nguyen [1], Yi-Hsuan Chiu, Jing- Mei Li, Yung-Jung Hsu *

Department of Materials Science and Engineering, National Chiao Tung University, Hsinchu 30010, Taiwan

ARTICLE INFO

Article history:
Received 20 July 2015
Received in revised form
23 November 2015
Accepted 27 November 2015
Available online 10 December 2015

Keywords:
GaOOH nanorods
Au decoration
Photocatalytic methanol oxidation
Anode photocatalyst
DMFCs

ABSTRACT

We reported for the first time that GaOOH nanorods, which were prepared using a facile chemical precipitation method, may display noticeable photocatalytic activities toward methanol oxidation under light illumination, a significant revelation for demonstrating their use as the anode photocatalyst in the half-cell reaction of direct methanol fuel cells (DMFCs). The GaOOH nanorods were further decorated with Au nanoparticles to endow them with increasingly pronounced charge separation, which conduced to a remarkable enhancement in the photocatalytic performance. Time-resolved photoluminescence spectroscopy was employed to depict the charge transfer event across the interface of GaOOH/Au, from which a correlation between photocatalytic efficiency and interfacial charge dynamics was realized. By incorporating GaOOH nanorods into the traditional Pt-catalyzed half-cell reaction, a 12.7% increase in anodic current generation can be attained under light illumination, demonstrating the promising potential of GaOOH as a practical anode photocatalyst in DFMCs. A further enhancement in methanol oxidation current up to 70.8% can be achieved by employing Au-decorated GaOOH nanorods, which was attributed to the efficient charge carrier transfer rendered by the Au decoration. The current study delivers both fundamental and practical importance as it broadens the scope of electrocatalysts for fuel cells, specifically by introducing a new class of highly efficient photocatalysts for promoting electrochemical reactions.

1. Introduction

Fuel cells as feasible energy conversion devices have received considerable attention in academia and industry. In general, these devices employ Pt/carbon catalysts as the electrode to drive the specific electrochemical reactions, for example, methanol oxidation reaction at the anode of direct methanol fuel cells (DMFCs) and oxygen reduction reaction at the cathode of proton exchange membrane fuel cells (PEMFCs) [1,2]. To achieve good dispersion and thus high stability of Pt, carbon supports with developed pore structures, high surface areas as well as excellent electrical conductivity are highly desirable. However, carbon supports serve merely the structural function and do not benefit the electrocatalytic activity. Therefore, it is necessary to explore stable non-carbon alternatives as the catalyst support in order to enhance the fuel cell durability and reliability. The introduction of novel support materials with co-catalytic functionality has proven to be an effective approach for improving both the activity and durability of Pt-based catalysts [3–10]. Transition metal oxides such as TiO_2 are one class of non-carbon materials that offer great promise as alternative catalyst supports for DMFCs because of the superior chemical stability and increased CO tolerance, the two determinant factors affecting the cell performance [11–15]. In particular, the introduction of TiO_2 may boost the performance of DMFCs by providing additional charge carriers for participation in anodic methanol oxidation under light illumination. In such a photocatalytic fuel cell (PFC) system, methanol oxidation at the anode is carried out electrocatalytically on Pt and photocatalytically on TiO_2. This configuration may substantially reduce the Pt usage yet still enhance the cell power output, which has significant implications from both the economical and practical points of view. However, the mediocre carrier utilization efficiency and low electrical conductivity of pure, un-modified TiO_2 have limited the cell performance enhancement when incorporated in DMFCs. As the addition of noble metals can effectively promote the carrier utilization and increase electrical conductivity for TiO_2 [16–18], metal-modified TiO_2 should function as a useful anode co-catalyst of DMFCs, especially when the cells operate under light illumination.

The search for highly active photocatalysts has been a challenging yet very important research topic due to the growing environmental concerns and increasing energy demand [19–22].

* Corresponding author. Fax: +886 3 5724724.
E-mail addresses: yhsu@cc.nctu.edu.tw, yhsu@mail.nctu.edu.tw (Y.-J. Hsu).
[1] These authors have contributed equally to this work.

http://dx.doi.org/10.1016/j.apcatb.2015.11.049
0926-3373/

Recently, a growing interest in employing p-block metal oxyhydroxides as practical photocatalysts has emerged [23–27]. As a representative example, GaOOH nanorods have demonstrated remarkable photocatalytic activities toward the degradation of aromatic compounds [28]. With the unique electronic configuration and geometric structures, GaOOH possesses many attributes favorable for photocatalytic applications. For example, due to the hybridization of broad sp orbitals, the conduction band of GaOOH is characterized by large dispersion, indicative of large mobility for the photoexcited electrons. Besides, the substantially low potential of valence band (+3.88 V vs. NHE) [28] offers GaOOH high oxidization power for performing various photocatalytic reactions. On the other hand, the primitive unit cell of GaOOH consists of distorted octahedral GaO_6 [29,30], which generates a strong dipole moment to facilitate charge separation. Despite these facts, the utility of GaOOH as a photocatalyst is quite limited and the exploitation of GaOOH remains an imperative task. In this work, we explored the photocatalytic properties of GaOOH nanorods toward methanol oxidation. The GaOOH nanorods were further decorated with Au nanoparticles to endow them with increasingly pronounced charge separation, an efficient strategy for advanced photocatalytic applications. The charge carrier separation at GaOOH/Au interface was investigated with time-resolved photoluminescence spectroscopy, from which a correlation between photocatalytic efficiency and interfacial charge dynamics was realized. Furthermore, the practical use of GaOOH nanorods as the anode co-catalyst in the half-cell reaction of DFMCs was also examined. To highlight the co-catalytic functionality of GaOOH, GaOOH nanorods were employed together with commercial Pt as the anode catalyst and the measurements of methanol electrocatalysis were carried out under light illumination. The results showed that incorporating GaOOH nanorods into the traditional Pt- catalyzed half-cell reaction led to a 12.7% increase in methanol oxidation current under light illumination, demonstrating the potential of GaOOH as a practical anode photocatalyst in DFMCs. A further enhancement in methanol oxidation current up to 70.8% can be achieved by employing Au- decorated GaOOH nanorods, which was ascribed to the efficient charge carrier transfer rendered by the Au decoration.

2. Experimental

2.1. Preparation of GaOOH nanorods

The synthesis was carried out in a chemical precipitation process. In the typical procedure, $Ga(NO_3)_3$ powder (128 mg, 5.0×10^{-4} mol) was dissolved in deionized water (15 mL) containing a given amount of HNO_3 (5 mL, 4.0 M). The pH of the mixed solution was adjusted to 7.0 using 1.0 M NaOH. The reaction solution was stirred at 80 °C for 24 h, producing a white dispersion of GaOOH nanorods. The product was collected by centrifugation, washed with deionized water and ethanol, and then dried in vacuum for later use.

2.2. Preparation of Au-decorated GaOOH nanorods

The decoration of Au nanoparticles on GaOOH nanorods was carried out using a chemical reduction method [31]. Briefly, GaOOH nanorods of 6 mg were dispersed in the reaction solution containing 60 mL of deionized water, 30 mL of ethanol and 600 μL of NaOH solution (0.1 M), followed by the addition of a desirable amount of $HAuCl_4$ solution (10 mM). After stirred at 30 °C for 30 min, the suspension was centrifuged, washed, and then dried in vacuum for later use. In this work, three different volumes of $HAuCl_4$ solution were employed to produce Au-decorated GaOOH nanorods (denoted as GaOOH/Au nanorods) with increasing Au contents. From the energy dispersive X-ray spectrometry (EDS) analysis, the content of Au deposited on GaOOH nanorods was respectively determined to be 0.5, 1.0 and 2.0 mol%. The thus-obtained samples were respectively denoted as GaOOH/Au-0.5, GaOOH/Au-1.0 and GaOOH/Au-2.0.

2.3. Time-resolved photoluminescence measurement

Time-resolved photoluminescence (PL) spectra were measured using a home-built single photon counting system (Horiba Jobin Yvon) which delivers an instrument response function down to 25 ps FWHM. A GaN diode laser ($\lambda = 375$ nm) with the pulse duration of 50 ps was used as the excitation source. The signals collected at the excitonic emission of coumarin 343 (denoted as C343, $\lambda_{em} = 482$ nm) were dispersed with a grating spectrometer, detected by a high-speed photomultiplier tube, and then correlated using a single photon counting card. Here, C343 (1.0×10^{-7} M) was used as an indicator dye to monitor the interfacial charge dynamics of the samples. By comparing the emission decay profile among different samples, the electron transfer event between GaOOH and Au for GaOOH/Au nanorods can be revealed. The recorded emission decay data were analyzed and fitted with a biexponential kinetics model $I(t) = A_1 e^{-t/\tau_1} + A_2 e^{-t/\tau_2}$, which generates two lifetime values, τ_1 and τ_2, and the corresponding amplitudes, A_1 and A_2. The intensity-average emission lifetime, $<\tau>$, was determined using the following expression $< \tau >= A_1{\tau_1}^2 + A_2{\tau_2}^2 / A_1\tau_1 + A_2\tau_2$. All the fitting results are summarized in Table 1.

2.4. Electrochemical measurement

Electrochemical measurements were conducted in a three-electrode cell using Pt as a counter electrode and Ag/AgCl as a reference electrode. The commercial carbon-supported Pt catalyst (denoted as Pt/C, Aldrich, 20 wt% of Pt) was suspended in an ethanol solution (1 mg/1 mL) containing 0.1 wt% nafion. Afterwards, the Pt/C suspension (100 μL) was spread and air-dried on carbon cloth substrate. Once completely dried, an aqueous suspension of GaOOH nanorods (100 μL, 1 mg/1 mL) was added dropwise with a microsyringe onto the carbon cloth, followed by an annealing treatment at 150 °C in air for 2 h to produce the composite catalyst of Pt/C-GaOOH. In this study, cyclic voltammetry (CV) was used to determine the activity of the samples toward methanol electrocatalysis. The CV profile was recorded in a N_2-saturated 0.5 M KOH electrolyte in the presence of 1.0 M methanol. The scan potential ranged from −0.8 V to 0.4 V and the scan rate was set at 20 mV/s. To highlight the co-catalytic effect of GaOOH, white light irradiation (xenon lamp, 100 mW/cm^2) was applied during the CV scan of composite catalyst.

2.5. Characterizations

The morphology and dimensions of the samples were examined with a field-emission scanning electron microscope (FESEM, JEOL, JSM-6500F) and a high-resolution transmission electron microscope (HRTEM, JEOL, JEM-3000). The crystallographic structure of the samples was investigated with X-ray diffraction (XRD, MAC Science, MXP18). The elemental analysis was conducted with EDS, the accessory of JSM-6500F and JEM- 3000. The chemical states of the samples were obtained with X-ray photoelectron spectroscopy (XPS, VG Scientific, Microlab 350), which was performed using Mg Kα ($h\upsilon = 1253.6$ eV) as X-ray source under a base pressure of 1.0×10^{-9} Torr. The UV–vis absorption spectra were collected using a Hitachi U-3900H spectrophotometer. The diffuse reflectance spectra were measured by Hitachi U-3900H with integrating sphere attachment. For steady-state PL spectroscopy, a Hitachi F-4500 equipped with a 150 W xenon lamp was used.

Table 1
Fitting results for emission decay profiles of C343 in the presence of different samples.

Entry I	A_1	τ_1 (ns)	A_2	τ_2 (ns)	<τ> (ns)	χ^2	k_{et} (s^{-1})
C343	11000	3.82	361	0.39	3.81	2.26	–
C343/GaOOH	9200	3.63	981	0.37	3.59	2.20	0.16×10^7 (C343 → GaOOH)[a]
C343/Au-0.5	10986	3.81	364	0.39	3.80	2.28	0.06×10^7 (C343 → Au-0.5)[a]
C343/Au-1.0	10985	3.81	370	0.39	3.80	2.00	0.06×10^7 (C343 → Au-1.0)[a]
C343/Au-2.0	10990	3.81	363	0.39	3.80	2.07	0.06×10^7 (C343 → Au-2.0)[a]
Entry II							
C343/GaOOH/Au-0.5	8180	3.39	2810	0.37	3.28	2.30	2.59×10^7 (GaOOH → Au-0.5)[b]
C343/GaOOH/Au-1.0	7950	3.00	2850	0.36	2.89	2.38	6.70×10^7 (GaOOH → Au-1.0)[b]
C343/GaOOH/Au-2.0	8230	3.57	1642	0.38	3.51	2.19	0.67×10^7 (GaOOH → Au-2.0)[b]

[a] The value was calculated by the expression $k_{et}(C343 \rightarrow A) = 1/\tau\left(C343/A\right) - 1/\tau(C343)$, where A = GaOOH, Au-0.5, Au-1.0 or Au-2.0.

[b] The value was calculated by the expression $k_{et}(GaOOH \rightarrow B) = 1/\tau\left(C343/GaOOH/B\right) - 1/\tau\left(C343/GaOOH\right) - k_{et}(C343 \rightarrow B)$, where B = Au-0.5, Au-1.0 or Au-2.0.

All of the absorption and emission spectra were recorded at room temperature under ambient atmosphere.

3. Results and discussion

3.1. Structural investigation

Fig. 1 shows the SEM image, XRD pattern and XPS analysis for GaOOH nanorods obtained in the chemical precipitation process. These pristine nanorods had a typical diameter of 90–120 nm and length up 1.0 μm. The corresponding XRD pattern can be indexed as the orthorhombic phase of GaOOH. On the other hand, the O 1s XPS spectrum of GaOOH nanords displayed two major chemical states: the O_1 component at 529.5 eV, which was assigned to the lattice oxygen species (Ga^{3+}–O), and the O_2 component at 531.3 eV, corresponding to the surface-adsorbed hydroxides (Ga–OH) [32]. In addition, the Ga XPS spectrum of Fig. S1 (see Supplementary data) exhibited signals corresponding to the bulk GaOOH with the binding energies of 1148.7 and 1121.7 eV for Ga $2p_{1/2}$ and Ga $2p_{3/2}$ core levels [28,33], respectively. Fig. 2 presents the structural investigations on GaOOH nanorods after they were reacted with $HAuCl_4$ in the chemical reduction process. Evidently, nanoparticles with a size of 8–10 nm were present on the nanorod surface. The HRTEM image taken at the interface of nanorod and nanoparticle regions clearly revealed two distinct sets of lattice fringes. The observed interlayer distances were consistent with the lattice spacings of orthorhombic GaOOH and fcc Au. The EDS element-mapping data further confirmed the successful decoration of Au nanoparticles on the surface of GaOOH nanorods. Importantly, as increasing the amount of $HAuCl_4$ employed, the number of Au nanoparticles deposited on GaOOH nanorods increased accordingly. This feasibility enabled the further manipulation on the photocatalytic performance of GaOOH because carrier utilization efficiency was highly dependent on the Au content [34–36].

3.2. Charge carrier dynamics of GaOOH/Au nanorods

Owing to the difference in band structure, the surface-decorated Au may function as an effective electron acceptor for GaOOH nanorods to promote charge carrier separation. Under light illumination, the photoexcited electrons of GaOOH would preferentially transfer to Au, leaving photogenerated holes at GaOOH to achieve charge separation. The charge transfer event between GaOOH and Au can be probed with PL spectroscopy by monitoring the interfacial charge dynamics of the samples. In this work, an indicator dye [37,38], C343, was used as the probe molecule to explore the charge carrier dynamics of GaOOH/Au nanorods. During the measurement, the variation of PL intensity and emission lifetime of C343 may give insightful information for evaluating the fate of charge carriers following light irradiation. Fig. 3(a) shows the steady-state PL spectra of C343 under different experimental conditions. When a given amount of pristine GaOOH nanorods was dispersed in C343 (sample was denoted as C343/GaOOH), the PL intensity of C343 was quenched. The PL quenching of C343 became more significant as a commensurate amount of GaOOH/Au nanorods was added (sample was denoted as C343/GaOOH/Au). The observed PL quenching of C343 for C343/GaOOH and C343/GaOOH/Au was attributed to the prevalence of charge separation under light illumination. Because GaOOH has a lower conduction potential (−0.87 V vs. NHE) [28] than the lowest-unoccupied molecular orbital (LUMO) potential of C343 (−1.23 V vs. NHE) [38], the photoexcited electrons of C343 were preferentially transported to GaOOH, leading to the depletion of free electrons for C343 and the subsequent depression of its PL. When Au was present on GaOOH nanorods, the photoexcited electrons of C343 may further transfer to Au through the GaOOH/Au interface because Au has a Fermi level (+0.50 V vs. NHE) [39] much lower than the conduction band potential of GaOOH. This situation caused a higher extent of free electron depletion for C343, which was accountable for the more significant PL quenching observed for C343/GaOOH/Au. On the other hand, the PL of C343 was not quenched in the presence of pure Au, implying that the electronic interaction of C343 with Au was insignificant. This observation supported the contention that the more significant PL quenching of C343 for C343/GaOOH/Au mainly originated from the further electron transfer from GaOOH to Au.

Time-resolved PL measurements were further conducted to explore the charge transfer event across the interface of GaOOH/Au. Fig. 3(b) compares the time-resolved PL spectra of C343 for five relevant samples. All of the emission decay profiles were fitted with a biexponential model to derive two decay components. The intensity-average lifetimes were then calculated and compared. As noted in Table 1, C343/GaOOH displayed a shorter emission lifetime (<τ> = 3.59 ns) than pure C343 (<τ> = 3.81 ns) did, suggesting the emergence of a nonradiative pathway from the electronic interaction between C343 and GaOOH. This suggestion was supported by the PL quenching of C343 observed for C343/GaOOH. Assuming that electron transfer from C343 to GaOOH dictated the emission decay of C343/GaOOH, the electron-transfer rate constant (k_{et}) from C343 to GaOOH can be calculated by the expression k_{et} (C343 → GaOOH) = (1/<τ>)(C343/GaOOH) − (1/<τ>)(C343) [40,41], approximately 0.16×10^7 s^{-1}. The Au decoration effect on the charge carrier transfer of GaOOH can be further depicted by inspecting the corresponding lifetime variation of C343. When Au of 0.5 mol% was present on GaOOH nanorods, the shrinkage of C343 emission lifetime became more noticeable (<τ> = 3.28 ns). It should be noticed that the emission lifetime of C343 in the presence of Au was fairly close to the value of pure C343, verifying the relatively insignificant electronic interaction of C343 with Au. Given that the electronic interaction between C343 and Au was quite minor, we ascribed the C343 emission lifetime short-

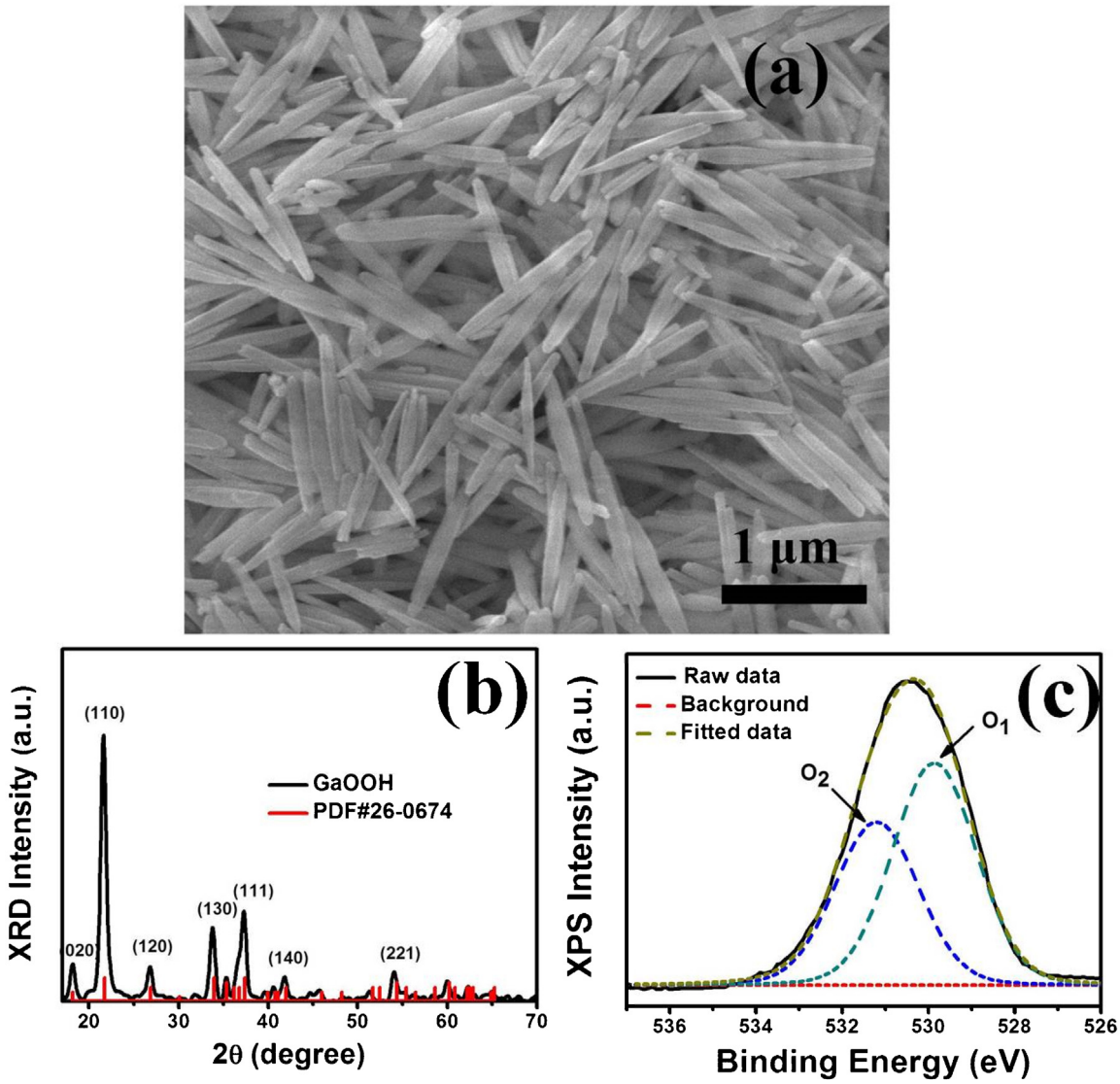

Fig. 1. (a) SEM image, (b) XRD pattern and (c) O 1s XPS spectrum of pristine GaOOH nanorods. In (b), the standard pattern of orthorhombic GaOOH was included for comparison.

ening of C343/GaOOH/Au-0.5 to the further electron transfer from GaOOH to Au. By comparing the average lifetime of C343 between C343/GaOOH/Au-0.5 and C343/GaOOH and deducting the contribution of electron transfer from C343 to Au, we obtained k_{et} (GaOOH → Au-0.5) as $2.59 \times 10^7\ s^{-1}$. This value was one order of magnitude larger than k_{et} (C343 → GaOOH), corroborating that Au functioned as an effective electron acceptor for GaOOH, further leading to increasingly pronounced charge separation as revealed in the much PL quenching of C343/GaOOH/Au. Similar to the cases of In_2O_3–TiO_2–Pt [41] and ZnSe·0.5(N_2H_4)-Au [42], Au as an electron acceptor in the current GaOOH/Au system had a quantitative effect on the mediation of interfacial charge transfer. As evident in Fig. 3(b), when the Au content of GaOOH/Au nanorods increased from 0.5 to 1.0 mol%, the emission lifetime of C343 was reduced from 3.28 to 2.89 ns. This lifetime reduction signified that Au of 1.0 mol% attracted more photoexcited electrons from GaOOH with an electron-transfer rate constant of $6.70 \times 10^7\ s^{-1}$. However, further increasing the Au content to 2.0 mol% caused a lengthened emission lifetime of C343 ($\langle\tau\rangle = 3.51$ ns), suggesting that charge carrier separation at the GaOOH/Au interface became decreasingly significant as Au of 2.0 mol% was present. The corresponding electron-transfer rate constant was estimated to be $0.67 \times 10^7\ s^{-1}$. The decrease of electron-transfer rate constant for GaOOH/Au-2.0 can be traced to the detrimental influence from the excess Au, which possibly acted as electron–hole recombination centers to alleviate the overall charge separation [41].

3.3. Photocatalytic properties

To demonstrate the promise for practical use, the present GaOOH/Au nanorods were applied as the photocatalyst for methanol oxidation, a critical anode reaction in DMFCs. A colorimetric approach was first used to quantify the methanol oxidation efficiency of the samples. Upon reacting with photogenerated holes, methanol may undergo oxidation to form formaldehyde [43], which can further react with acetylacetone and excess ammonium acetate to generate a yellow colored product diacetyldihydrolutidine (denoted as DDL). As Fig. 4(a) shows, by measuring the corresponding absorbance at 404 nm, the formation of DDL can be quantitatively characterized, which offers a direct index to evaluate the methanol oxidation efficiency. Fig. 4(b) presents the formation of DDL as a function of irradiation time over different

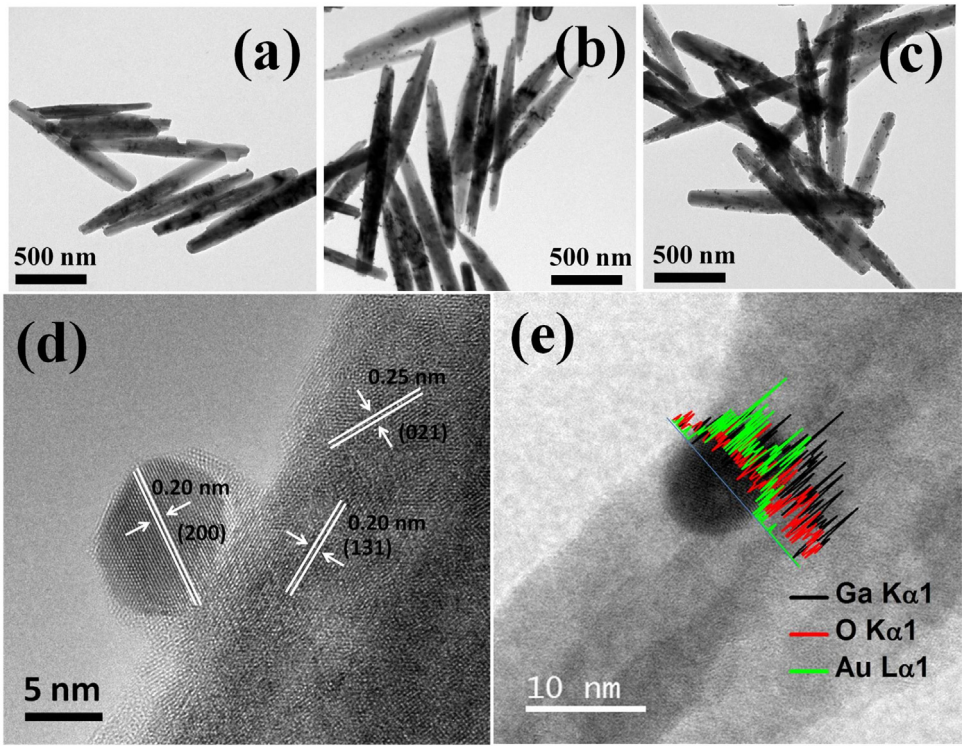

Fig. 2. TEM images of Au-decorated GaOOH nanorods with Au contents of (a) 0.5, (b) 1.0 and (c) 2.0 mol%. (d) and (e) show the corresponding HRTEM image and TEM-EDS analysis, respectively.

samples. We observed two important features as stated below. First, all the three GaOOH/Au samples performed better toward methanol photooxidation than pristine GaOOH nanorods did. This superiority was ascribed to the decorated Au that promoted the overall charge separation by accepting photoexcited electrons from GaOOH, therefore providing more photogenerated holes for methanol oxidation. It might be argued that the plasmonic effect of Au may contribute to the enhanced photocatalytic activity of GaOOH/Au. Here we evaluated such possibility using absorption spectroscopy. As displayed in Fig. S2 (see Supplementary data), the three GaOOH/Au samples did not show noticeable absorption band that could be assigned to the surface plasmon resonance of Au. This phenomenon can be interpreted by the relatively low contents of the decorated Au. Since the surface plasmon resonance was rather insignificant, the plasmonic effect and its involvement in the photocatalysis for the present GaOOH/Au nanorods can be ruled out at the current stage. Second, among the three GaOOH/Au nanorods tested, GaOOH/Au-1.0 displayed the highest photocatalytic efficiency for methanol oxidation. This observation was consistent with the results of charge carrier dynamics, in which GaOOH/Au-1.0 attained the largest electron-transfer rate constant and was therefore expected to possess the highest number of charge carriers available for methanol oxidation. The carrier dynamics data showed that charge separation efficiency of GaOOH/Au-2.0 became less significant, ascribable to the counteraction effect associated with interfacial electron–hole recombination. When the Au content was increased to 2.0 mol%, electrons accumulated in Au were substantially abundant such that the photogenerated holes in GaOOH might be attracted and transported to Au [31,39]. The subsequent interfacial electron–hole recombination would lead to the depletion of photoexcited charge carriers and thus the depression of photocatalytic activity as observed. On the other hand, the stability is another important parameter for evaluating the practical use of photocatalysts. To consider this property, we further performed

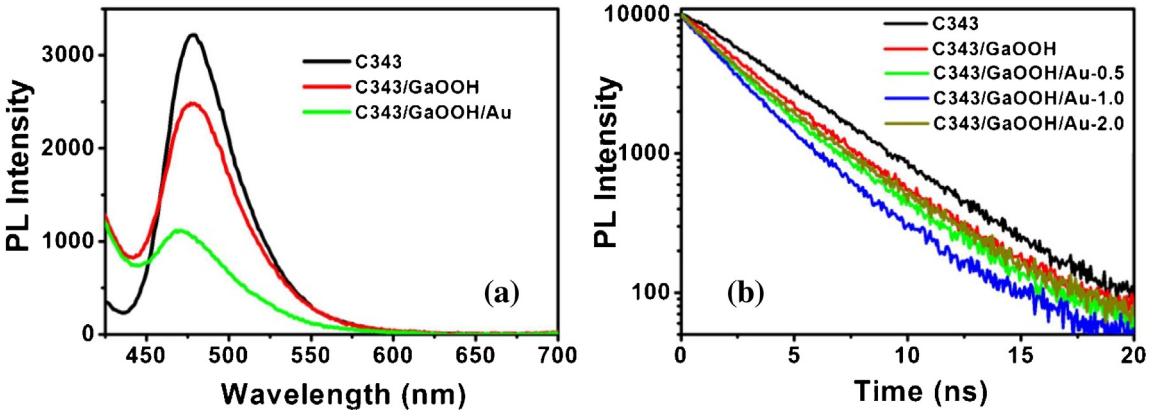

Fig. 3. (a) Steady-state PL spectra and (b) time-resolved PL spectra of C343 in the presence of different samples.

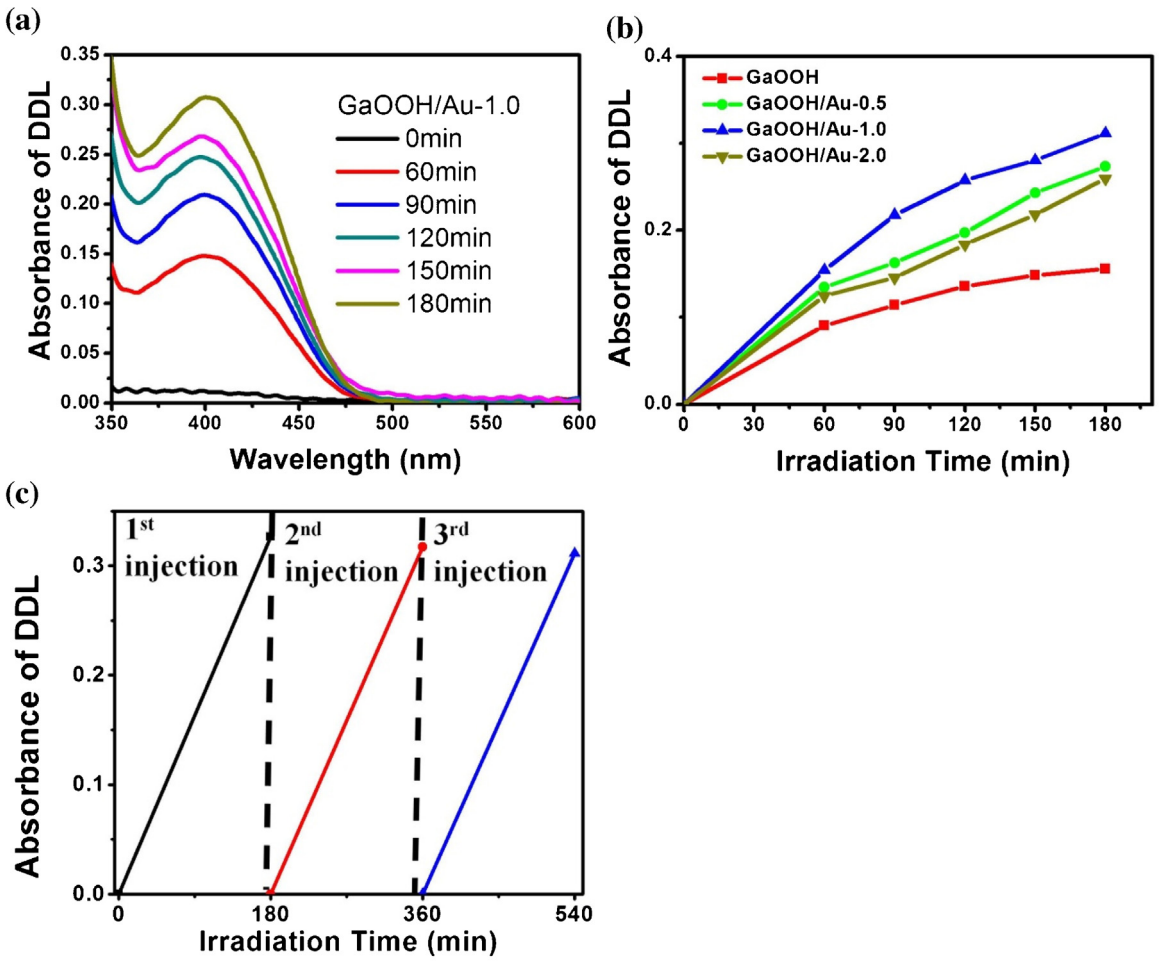

Fig. 4. (a) Absorption spectra of DDL under different irradiation times by using GaOOH/Au nanorods. (b) Variation of DDL absorbance with irradiation time for different samples. (c) Recycling test on GaOOH/Au-1.0 sample for DDL formation.

a reusability test by using GaOOH/Au-1.0 as the representative photocatalyst. As shown in Fig. 4(c), a slight decay in photocatalytic activity was found for GaOOH/Au-1.0 after repeatedly used in methanol photooxidation for three cycles. This gradual activity decline was related to the inevitable sample loss during the centrifugation-collection process at each cycle. The demonstration from stability test revealed that the present GaOOH/Au nanorods did not suffer from significant deactivation in the multiple recycling usages for methanol oxidation, which is an essential attribute for the long-term photocatalytic applications.

To illustrate the potential as an anode co-catalyst of DFMCs, GaOOH/Au nanorods were further employed with commercial Pt catalyst in the anodic half-cell reaction. Note that there has been a growing interest in exploiting alkaline DMFCs since the activity of Pt catalysts as well as the CO tolerance can be substantially improved in the alkaline environment [44,45]. The development of highly efficient alkaline DMFCs has thus been imperative. Fig. 5 compares the CVs of methanol oxidation recorded in alkaline media on five relevant samples with and without light irradiation. All the samples showed a typical CV profile of methanol electrocatalysis with two characteristic oxidation peaks. The forward peak at −0.20 V (vs. Ag/AgCl) corresponded to the oxidation of methanol, and the backward peak around −0.35 V (vs. Ag/AgCl) originated from the oxidation of intermediate carbonaceous species [46]. For the commercial Pt/C catalyst, a forward peak current density of 5.20 mA/cm^2 was recorded. When employing GaOOH nanorods together with Pt/C as the anode catalyst (denoted as Pt/C-GaOOH), a comparable peak current of methanol oxidation was obtained in the dark. Nevertheless, an evident suppression in the backward peak current was noticed, suggesting that CO tolerance of the composite catalyst Pt/C-GaOOH was enhanced. Here, we surmised that GaOOH may affect the methanol electrocatalysis by facilitating the removal of the adsorbed carbonaceous species. According to the XPS result in Fig. 1(c), the surfaces of GaOOH nanorods contained abundant hydroxide groups. These hydroxides may function as activated oxygen moieties for the oxidation of carbonaceous species, thereby expediting their removal from the catalyst surface to improve the CO tolerance [47]. The co-catalytic effect of GaOOH introduction on methanol electrocatalysis can be further revealed by applying light irradiation during the CV scans. As noticed in Fig. 5, the composite catalyst of Pt/C-GaOOH showed an enhanced peak current of methanol oxidation (5.86 mA/cm^2) under light illumination, which was around 12.7% improvement over commercial Pt/C. The participation of photoexcited charge carriers from GaOOH nanorods in methanol oxidation may account for such a current enhancement. Considering that the carrier utilization efficiency of pristine GaOOH was low, the performance enhancement achieved by Pt/C-GaOOH should be quite limited as was observed. With the employment of GaOOH/Au-1.0, the enhancement of methanol oxidation current can therewith reach up to 70.8% (8.88 mA/cm^2 for Pt/C-GaOOH/Au-1.0). Note that the increasingly pronounced charge carrier separation for GaOOH/Au-1.0, in which the photoexcited electrons preferentially transferred to Au and the photogenerated holes were mostly localized at GaOOH,

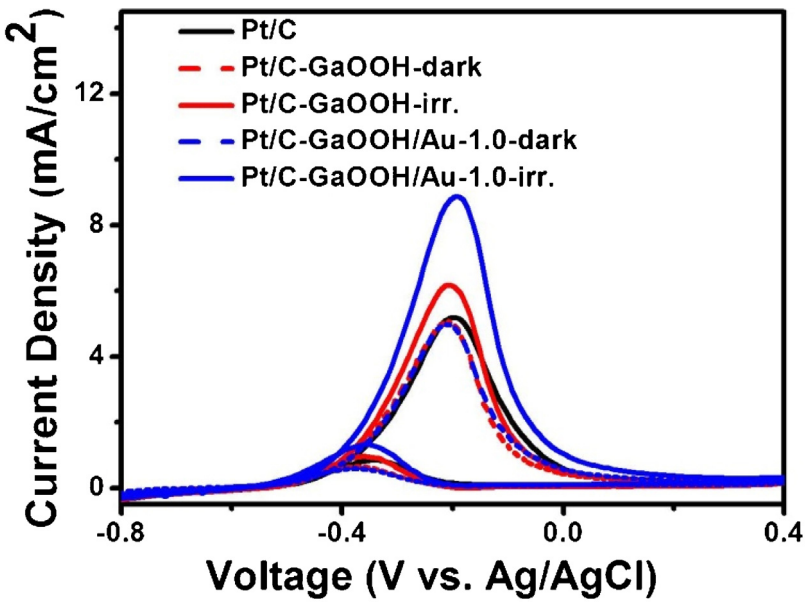

Fig. 5. CVs of methanol oxidation on commercial Pt/C, composite Pt/C-GaOOH and Pt/C-GaOOH/Au- 1.0 catalysts with and without light irradiation.

was particularly favourable for promoting methanol electrocatalysis. Under this circumstance, the electrons accumulated at Au would transfer readily to the external circuit via the carbon support, while the photogenerated holes localized at GaOOH may effectively oxidize methanol to generate additional electrons. As a result of such an efficient charge carrier transfer, the composite catalyst Pt/C-GaOOH/Au-1.0 can achieve a substantially enlarged current of methanol oxidation.

4. Conclusions

In conclusion, we presented the photocatalytic properties of GaOOH/Au nanorods toward methanol oxidation and successfully demonstrated their use as the anode photocatalyst in the half-cell reaction of DFMCs. The results showed that incorporation of GaOOH/Au nanorods not only improved the CO tolerance for the commercial Pt/C catalyst, but also enhanced the anodic current generation of DFMCs under light illumination. The intriguing electronic and geometric features of GaOOH, i.e., the substantially low valence band potential and pronounced charge separation, make the present GaOOH/Au nanorods especially promising in technologically important photoconversion fields, such as photocatalytic oxygen evolution and oxidative reforming of organics. The demonstrations from this work also facilitate the utilization of GaOOH as efficient photoelectrodes as well as stable catalyst supports with co-catalytic functionality in relevant electrochemical and photoelectrochemical devices.

Acknowledgment

This work was financially supported by the Ministry of Science and Technology of Taiwan under grants NSC-102-2113-M-009-005-MY2 and MOST 104-3113 -E-009-001.

Appendix A. Supplementary data

Supplementary data associated with this article can be found, in the online version, at http://dx.doi.org/10.1016/j.apcatb.2015.11.049.

References

[1] H. Liu, C. Song, L. Zhang, J. Zhang, H. Wang, D.P. Wilkinson, J. Power Sour. 155 (2006) 95–110.
[2] K. Sundmacher, Ind. Eng. Chem. Res. 49 (2010) 10159–10182.
[3] S. Liao, K.A. Holmes, H. Tsaprailis, V.I. Birss, J. Am. Chem. Soc. 128 (2006) 3504–3505.
[4] V. Mazumder, Y. Lee, S. Sun, Adv. Funct. Mater. 20 (2010) 1224–1231.
[5] P. Wu, H. Zhang, Y. Qian, Y. Hu, H. Zhang, C. Cai, J. Phys. Chem. C 117 (2013) 19091–19100.
[6] J.J. Wang, Y.T. Liu, I.L. Chen, Y.W. Yang, T.K. Yeh, C.H. Lee, C.C. Hu, T.C. Wen, T.Y. Chen, T.L. Lin, J. Phys. Chem. C 118 (2014) 2253–2262.
[7] Z. Qiu, H. Huang, J. Du, T. Feng, W. Zhang, Y. Gan, X. Tao, J. Phys. Chem. C 117 (2013) 13770–13775.
[8] L. Li, J. Zhang, Y. Liu, W. Zhang, H. Yang, J. Chen, Q. Xu, ACS Sustain. Chem. Eng. 1 (2013) 527–533.
[9] J. Jiang, A. Kucernak, J. Electroanal. Chem. 543 (2003) 187–199.
[10] H. Möller, P.C. Pistorius, J. Electroanal. Chem. 570 (2004) 243–255.
[11] P.A. Mandelbaum, A.E. Regazzoni, M.A. Blesa, S.A. Bilmes, J. Phys. Chem. B 103 (1999) 5505–5511.
[12] K. Drew, G. Girishkumar, K. Vinodgopal, P.V. Kamat, J. Phys. Chem. B 109 (2005) 11851–11857.
[13] C. Gu, C. Shannon, J. Mol. Catal. A: Chem. 262 (2007) 185–189.
[14] C. Jia, H. Yin, H. Ma, R. Wang, X. Ge, A. Zhou, X. Xu, Y. Ding, J. Phys. Chem. C 113 (2009) 16138–16143.
[15] L. Yang, Y. Xiao, G. Zeng, S. Luo, S. Kuang, Q. Cai, Energy Fuels 23 (2009) 3134–3138.
[16] H.J. Kim, D.Y. Kim, H. Han, Y.G. Shul, J. Power Sour. 159 (2006) 484–490.
[17] T.D. Dzhafarov, S.A. Yuksel, M. Aydin, Mater. Sci. Appl. 5 (2014) 1020–1026.
[18] M. Haruta, M. Daté, Appl. Catal. A: Gen. 222 (2001) 427–437.
[19] M.-Q. Yang, N. Zhang, M. Pagliaro, Y.-J. Xu, Chem. Soc. Rev. 43 (2014) 8240–8254.
[20] C. Han, Z. Chen, N. Zhang, J.C. Colmenares, Y.-J. Xu, Adv. Funct. Mater. 25 (2015) 221–229.
[21] N. Zhang, M.-Q. Yang, S. Liu, Y. Sun, Y.-J. Xu, Chem. Rev. 115 (2015) 10307–10377.
[22] S. Liu, Z.-R. Tang, Y. Sun, J.C. Colmenares, Y.-J. Xu, Chem. Soc. Rev. 44 (2015) 5053–5075.
[23] M. Muruganandham, R. Amutha, M.S.M. Abdel Wahed, B. Ahmad, Y. Kuroda, R.P.S. Suri, J.J. Wu, M.E.T. Sillanpää, J. Phys. Chem. C 116 (2012) 44–53.
[24] S. Fujihara, Y. Shibata, E. Hosono, J. Electrochem. Soc. 152 (2005) C764–C768.
[25] H.S. Qian, P. Gunawan, Y.X. Zhang, G.F. Lin, J.W. Zheng, R. Xu, Cryst. Growth Des. 8 (2008) 1282–1287.
[26] Y.C. Zhang, X. Wu, X.Y. Hu, Q.F. Shi, Mater. Lett. 61 (2007) 1497–1499.
[27] S.G. Chen, S.M. Luo, Y. Zhou, Y. Chen, Y.Q. Liu, C.G. Long, Mater. Lett. 62 (2008) 4566–4569.
[28] M. Sun, D. Li, W. Zhang, X. Fu, Y. Shao, W. Li, G. Xiao, Y. He, Nanotechnology 21 (2010) 355601.
[29] Y. Inoue, Energy Environ. Sci. 2 (2009) 364–386.
[30] J. Sato, H. Kobayyashi, Y. Inoue, J. Phys. Chem. B 107 (2003) 7970–7975.
[31] Y.-C. Pu, Y.-C. Chen, Y.-J. Hsu, Appl. Catal. B: Environ. 97 (2010) 389–397.
[32] F. Conrad, M. Bauer, D. Sheptyakov, S. Weyeneth, D. Jaeger, K. Hametner, P.-E. Car, J. Patscheider, D. Günther, G.R. Patzke, RSC Adv. 2 (2012) 3076–3082.

[33] M.I. Dar, S. Sampathc, S.A. Shivashankar, RSC Adv. 4 (2014) 49360–49366.
[34] H. Li, Zh. Bian, J. Zhu, Y. Huo, H. Li, Y. Lu, J. Am. Chem. Soc. 129 (2007) 4538–4539.
[35] Y. Wu, H. Liu, J. Zhang, F. Chen, J. Phys. Chem. C 113 (2009) 14689–14695.
[36] S. Liu, Y.-J. Xu, Nanoscale 5 (2013) 9330–9339.
[37] S. Yu, S.Y. Lee, J. Yeo, J.W. Han, J. Yi, J. Phys. Chem. C 118 (2014) 29583–29590.
[38] Y.-C. Pu, W.-H. Lin, Y.-J. Hsu, Appl. Catal. B: Environ. 163 (2015) 343–351.
[39] W.-T. Chen, Y.-J. Hsu, Langmuir 26 (2010) 5918–5925.
[40] G. William, P.V. Kamat, Langmuir 25 (2009) 13869–13873.
[41] Y.-C. Chen, Y.-C. Pu, Y.-J. Hsu, J. Phys. Chem. C 116 (2012) 2967–2975.
[42] Y.-C. Chen, T.-C. Liu, Y.-J. Hsu, ACS Appl. Mater. Interfaces 7 (2015) 1616–1623.
[43] T. Nash, Biochem. J. 55 (1953) 416–421.
[44] A.V. Tripkovíc, K.D. Popovíc, B.N. Grgur, B. Blizanac, P.N. Ross, N.M. Markovíc, Electrochim. Acta 47 (2002) 3707–3714.
[45] J.S. Spendelow, G.Q. Lu, P.J.A. Kenis, A. Wieckowski, J. Electronanal. Chem. 568 (2004) 215–224.
[46] W.-T. Chen, Y.-K. Lin, T.-T. Yang, Y.-C. Pu, Y.-J. Hsu, Chem. Commun. 49 (2013) 8486–8488.
[47] P.A. Adcock, S.V. Pacheco, K.M. Norman, F.A. Uribe, J. Electrochem. Soc. 152 (2005) A459–A466.